Scripta Materialia 161 (2019) 74–77

Contents lists available at ScienceDirect

Scripta Materialia

journal homepage: www.elsevier.com/locate/scriptamat

Effect of volume fraction of gradient nanograined layer on high-cycle fatigue behavior of Cu

Lijun Jing [a,b], Qingsong Pan [a], Jianzhou Long [a], Nairong Tao [a], Lei Lu [a,*]

[a] Shenyang National Laboratory for Materials Science, Institute of Metal Research, Chinese Academy of Sciences, Shenyang 110016, PR China
[b] School of Materials Science and Engineering, University of Science and Technology of China, Hefei 230026, PR China

ARTICLE INFO

Article history:
Received 18 September 2018
Received in revised form 16 October 2018
Accepted 16 October 2018
Available online xxxx

Keywords:
Gradient nanograin (GNG)
Copper
The fatigue endurance limit
Cyclic deformation
Abnormal grain coarsening

ABSTRACT

Fatigue behaviors of two Cu samples with different volume fractions of gradient nanograined (GNG) surface layer, prepared by surface mechanical grinding treatment, are investigated under stress-controlled high-cycle fatigue tests. With increasing the volume fraction of GNG layer from 4.3% to 13%, the fatigue endurance limit (at 10^7 cycles) of GNG Cu is enhanced from 88 to 98 MPa, much higher than that of coarse grained counterpart. Large volume fraction of GNG layer effectively postpones the extension of abnormal grain coarsening from a deeper subsurface layer to the topmost surface and thereby retards the initiation of surface fatigue crack.

Compared with conventional homogeneous coarse-, ultrafine- or nano-grained (CG, UFG and NG) metals, gradient nanograined (GNG) metals, with grain sizes spatially increasing from nanoscale in surface to micron in core, exhibit high strength while maintaining considerable tensile ductility, due to the suppression of strain localization [1–3]. Moreover, high-cycle fatigue properties (such as the fatigue endurance limit at 10^7 cycles) of GNG metals under cyclic loading are enhanced as well, compared to their CG counterparts, primarily due to the presence of high-strength GNG layer, which retards the initiation of surface cracks [4–9]. For instance, the fatigue endurance limit of GNG 316L stainless steel is 320 MPa, remarkably higher than that of CG (180 MPa) [7].

As a typical hierarchical nanostructure, fatigue properties and cyclic deformation behaviors of GNG metals closely depend on their microstructure parameters such as volume fraction of GNG layer and grain size distributions, etc. [10]. It was shown that with increasing the spherical shot diameter of surface mechanical attrition treatment or decreasing the sample diameter, the fatigue endurance limit of GNG 316L stainless steel increases further, possibly because of a higher volume fraction of martensite and deformation twins formed in GNG layer and enhanced strength [4,7]. However, quantitative investigation of how the volume fraction of GNG layer influences the fatigue properties and cyclic deformation behaviors of GNG metals is still rather limited so far. This scarcity mainly stems from the difficulty in controllably preparing metals with GNG surface layer.

In this study, two pure Cu samples with different volume fractions of GNG surface layer are prepared by means of surface mechanical grinding treatment (SMGT) [11]. The cyclic deformation-induced microstructural evolution in the GNG layer and the volume fraction of GNG layer influencing the cyclic deformation behavior of GNG Cu are discussed.

Commercial-purity (99.98 wt%) Cu rods consisting of equiaxed micrometre-sized grains with an average grain size of 21 μm are machined into dog-bone-shaped samples with a gauge length of 12 mm and a gauge diameter of 6 mm. Both gauge sections and arc transitions are processed by SMGT at cryogenic temperature (~173 K) with liquid nitrogen [11]. During SMGT process, a hemispherical WC/Co tool tip with a radius of 6 mm penetrating into the ground sample induces plastic strain and structural refinement in its surface layer, but without material removal from the sample surface. Increasing the processing passes and penetration depth induce a larger accumulative plastic strain in a much thicker surface layer of the treated sample, resulting in a larger volume fraction of GNG layer. As designed, by adjusting 3 and 8 processing passes, the total penetration depths of tips on two sets of sample surface are about 120 and 320 μm, respectively.

The volume fraction of GNG layer (including NG and UFG layer) for GNG Cu can be expressed as

$$\mathrm{Vol}\% = \frac{\left[d_0^2 - (d_0 - 2t)^2\right]}{d_0^2} \times 100\% \quad (1)$$

where d_0 is the diameter of its gauge section (i.e. 6 mm), and t is the thickness of GNG layer (65 and 200 μm for the 3 and 8 passes sample,

* Corresponding author.
E-mail address: llu@imr.ac.cn (L. Lu).

https://doi.org/10.1016/j.scriptamat.2018.10.019
1359-6462/

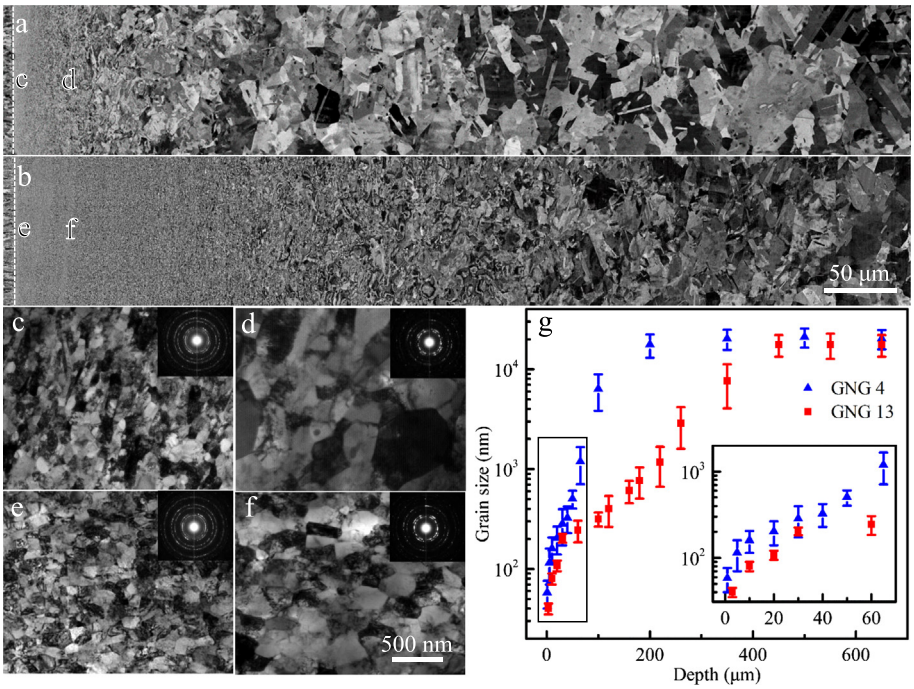

Fig. 1. Typical longitudinal-sectional SEM images of GNG 4 (a) and GNG 13 (b). The dashed line represents the treated surface. TEM images of microstructures (c–f) at positions c–f indicated in (a) and (b), respectively, and the insets in (c–f) are the selected area electron diffraction (SAED) patterns. Variation of average grain sizes along depth from the topmost surface (g). The inset in (g) is the amplified image of the rectangle.

see Fig. 1). The estimated volume fraction of GNG layer is about 4.3% and 13.0% for the 3 and 8 passes sample, which is hereafter referred to as GNG 4 and 13 samples, respectively.

Uniaxial tensile tests of both GNG Cu samples are performed on an Instron 5982 testing machine at a strain rate of 1×10^{-3} s^{-1}. A clip-on Instron extensometer is used to measure the tensile strain of the samples upon loading. Stress-controlled symmetric tension-compression fatigue tests of GNG Cu samples are performed on an Instron 8874 testing machine at ambient temperature. A sinusoidal wave with a frequency of 30 Hz is used. Specially, one set of GNG samples are cyclically deformed at stress amplitude ($\Delta\sigma/2$) of 140 MPa, but interrupted at the planned cycles (N) of loading (i.e. $N = 3.6 \times 10^4$, 8.7×10^4 cycles) before failure and then fully unloaded.

The longitudinal-sectional microstructures of GNG Cu in SMGT state and after fatigue tests are characterized via FEI Nova NanoSEM 430 field emission gun scanning electron microscope (SEM) with backscattered electron imaging. Detailed microstructures of GNG Cu are further investigated by FEI Tecnai F20 transmission electron microscope (TEM). Over 500 grains from numerous TEM images are measured to determine the average grain size in different depths of GNG layer. Three-dimensional surface features of GNG Cu fatigued to failure are investigated by Olympus LEXT OLS4100 confocal laser scanning microscope (CLSM).

An as-prepared GNG 4 sample shows shining surface with a minor surface roughness ($R_a \approx 0.26$ μm) and without cracks. Longitudinal SEM observations in Fig. 1a indicate a spatially gradient microstructure along the radial direction of GNG Cu rod sample, composed of a NG layer (with a depth of 5 μm in top surface layer), an UFG layer (at depth from 5 to 65 μm), a deformed CG layer and an undeformed CG core. Closer TEM images show that most NGs and UFGs are separated by curved grain boundaries (GBs) (Fig. 1c and d), which are evidently in a high-energy non-equilibrium state, analogous to those in nanostructured metals prepared by severe plastic deformation [12,13]. These grains are randomly oriented, as displayed by the selected-area electron diffraction (SAED) patterns (insets in Figs.1c and 1d).

As shown in Fig. 1b, GNG 13 sample exhibits a comparably minor surface roughness (0.32 μm) and similar gradient structure, but much thicker NG and UFG layer (20 and 180 μm), compared with that of GNG 4 (Fig. 1a). TEM observations show that UFGs and NGs of GNG 13 have identical morphologies to that of GNG 4 at the same depth, but with a relatively smaller grain size (Fig. 1c–g).

Tensile engineering stress-strain curves in Fig. 2a show a high yield strength (σ_y, at 0.2% offset) of 123 ± 4 MPa for GNG 4, twice that of CG counterparts. With increasing volume fraction of GNG layer from 4.3% to 13%, σ_y of GNG 13 increases to 144 ± 4 MPa. The ultimate tensile strength (σ_{uts}) and uniform strain (δ_u) of both GNG samples are almost comparable to that of CG counterparts.

Stress-controlled fatigue results (S—N curve) in Fig. 2b show that the fatigue endurance limit (σ_{-1}) for GNG 4 is 88 MPa, much higher than that of CG Cu (56 MPa) and comparable with that of UFG Cu (~90 MPa) [14–17]. With increasing the volume fraction of the GNG layer from 4.3% to 13%, σ_{-1} increases to 98 MPa. Taking the sample fatigued at $\Delta\sigma/2$ of 140 MPa as an example, fatigue lives for GNG 4 and GNG 13 are approximately 7 and 15 times longer than that of CG counterparts fatigued at the same condition. These results clearly demonstrate that increasing the volume fraction of GNG surface layer on bulk CG metals effectively improves both the high-cycle fatigue life and the fatigue endurance limit under stress controlled fatigue tests.

To ascertain the influence of the volume fraction of the GNG surface layer on HCF behavior, longitudinal-sectional microstructural evolutions of both GNG Cu samples with increasing cycles at $\Delta\sigma/2 =$ 140 MPa are systematically investigated by SEM. Fig. 3a shows that after 3.6×10^4 cycles (corresponding to the fatigue-to-failure lifetime of CG Cu at the same $\Delta\sigma/2$), abnormal coarsened grains are detected in the subsurface layer (at a depth of ~30–40 μm) of GNG 4, before the occurrence of fatigue failure. With further increasing cycles, grain coarsening extends to the CG core and GNG top surface simultaneously (Fig. 3b), consistent with that in ref. [8]. At 1.8×10^5 cycles (fatigue-to-failure life of GNG 4), obviously abnormally coarsened grains with an average grain size of 7 μm appear here and there on the topmost surface (Fig. 3c and d).

However, no obvious microstructural change is detected for GNG 13 at 3.6×10^4 cycles, as shown in Fig. 3e. At 8.7×10^4 cycles, very

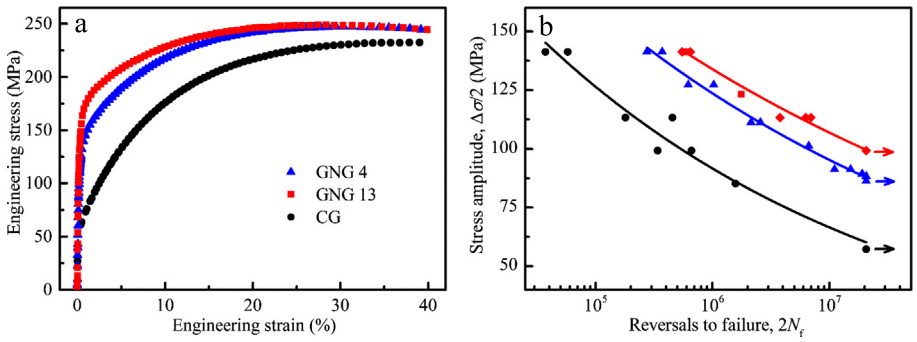

Fig. 2. Tensile engineering stress-strain curves (a) and cyclic stress amplitude-fatigue life curves (b) of GNG 4 and GNG 13 samples; "→" in (b) denotes the sample without failure. Fatigue data of GNG 13 in ref. [6] are also included.

tiny abnormal coarsened grains with a mean grain size of 2 μm are just observed at a depth of 50–70 μm (Fig. 3f). At 1.8×10^5 cycles (i.e. fatigue lifetime of GNG 4), more and more grain coarsening occurs in a larger region with a depth ranging from 110 to 20 μm (Fig. 3g), but does not extend to the top surface layer. After 2.9×10^5 cycles when GNG 13 is fatigued to failure, abnormal grain coarsening has reached the topmost surface (Fig. 3h and i).

Randomly distributed extrusions/intrusions (Fig. 4a and b) are observed on the surface of both GNG Cu fatigued to failure. The average altitude differences between the adjacent extrusions and intrusions for both GNG samples are comparable, approximately 0.54 μm (Fig. 4c and d). The fatigue feature of GNG Cu is analogous to the typical micron-scale extrusions/intrusions in fatigued CG metals [18–20], but different from the macroscopic shear bands in fatigued UFG or NG metals, which are mainly distributed at ~45° relative to the stress axis [14,15,21]. We have to emphasize here that no surface fatigue features are observed before 8.7×10^4 for GNG 4 and 1.8×10^5 cycles for GNG 13. In other words, surface extrusion/intrusions can be detected only after abnormal grain coarsening reaches the topmost surface of fatigued GNG Cu, demonstrating that they are only formed in abnormal coarse grains at the topmost surface as a result of dislocation activities, just like that observed in fatigued CG metals [18–20].

It is well accepted that the most fatigue damage or failures occur on the surface of samples/component and then propagate into interior region [19,22]. Here in this study, abnormal grain coarsening occurs in the subsurface UFG layer and then propagates to the top surface, suggesting that CG metals coated with a gradient nanostructured skin can effectively suppress the surface damage. It is mainly owing to the fact that since the yield strength of the subsurface UFG layer with relatively larger grain sizes is much lower than that of the NG layer, the cyclic plastic strain mainly concentrates in the subsurface UFG layer while the NG layer is still under elastic deformation, during small-amplitude cyclic deformation. From the experimental observations in Fig. 3, it can be found that when abnormal grain coarsening has reached the topmost surface of GNG 4 after 1.8×10^5 cycles, however, its position in fatigued GNG 13 is ~20 μm away from the topmost surface, which offers another 1.1×10^5 cycles for abnormal grains to reach the topmost surface. These analysis demonstrates that a higher volume fraction of GNG layer can effectively postpone the extension of abnormal grain coarsening to the topmost surface.

Moreover, the onset of abnormal grain coarsening in the subsurface layer of GNG 13 is also postponed by ~5×10^4 cycles, compared to GNG 4, possibly because the plastic strain sustained by GNG13 with a higher volume fraction of high-strength GNG layer is smaller than that of GNG 4 at the same stress amplitude. It is reasonably understandable that abnormally coarsened grains can only be detected in the subsurface layer of GNG 13 after a longer number of cycles, that is with accumulation of a larger plastic strain.

Comparison of microstructures of GNG 4 and GNG 13 before and after fatigue tests (Figs. 1 and 3) shows that although the initial

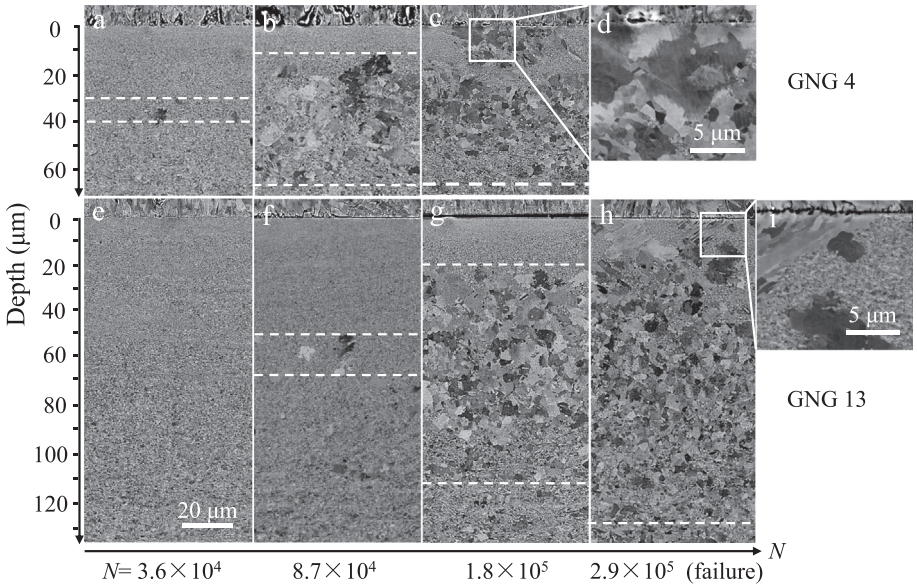

Fig. 3. Typical longitudinal-sectional SEM images of GNG 4 (a–d) and GNG 13 (e–i) fatigued at $\Delta\sigma/2 = 140$ MPa with different numbers of cycles (N): 3.6×10^4 (a, e), 8.7×10^4 (b, f), 1.8×10^5 (c, g), and 2.9×10^5 cycles (h). (d) and (i) are the amplified images of the white squares in c and h, respectively.

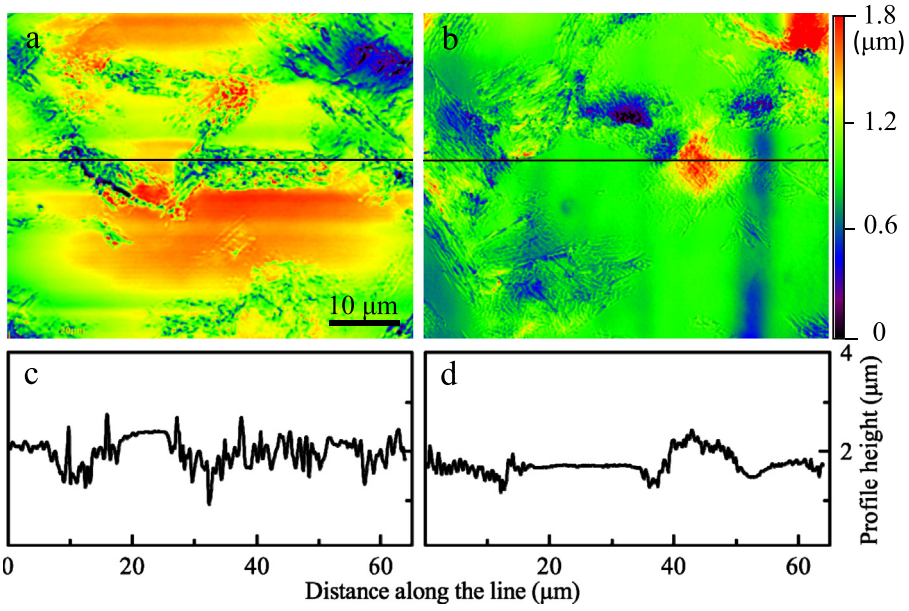

Fig. 4. Typical CLSM images of GNG4 (a) and GNG13 (b) fatigued to failure at $\Delta\sigma/2 = 140$ MPa; Surface fluctuations (c) and (d) along the black line in (a) and (b), respectively.

positions of abnormal grain coarsening for both GNG samples are different, their original sizes are similar, being about 200–300 nm. Coincidentally, this grain size is also the typical saturated value achieved by severe plastic deformation processes, such as equal-channel angular pressing [12]. The high energy state of UFGs with curved GBs and a high density of dislocations should act as the thermodynamic driving force to trigger the occurrence of abnormal grain coarsening in GNG Cu during cyclic loading. However, the underlying instability mechanism of UFG structure with the grain size of 200–300 nm during cyclic deformation is still worthy of in-depth study.

The high-cycle fatigue properties of metals with homogeneous microstructures under stress control are generally dominated by their σ_{uts}, following Basquin equation [19],

$$\frac{\Delta\sigma}{2} = \sigma_f'(2N_f)^b \tag{2}$$

where σ_f is the fatigue strength coefficient, which is close to σ_{uts}, and b is the fatigue strength exponent. A higher σ_{uts} usually results in a higher σ_{-1} and longer fatigue life at constant $\Delta\sigma/2$, as verified by fatigue data of UFG and CG metals [14,23]. Here, σ_{uts} of both GNG Cu samples are comparable to that of CG Cu, much smaller than that of UFG Cu. However, σ_{-1} of both GNG Cu samples are comparable to that of UFG, and much higher than that of CG counterparts. Specifically, σ_{-1} of GNG 13 is 10 MPa higher than that of GNG 4, although their σ_{uts} are nearly same.

In summary, both the high-cycle fatigue life and the fatigue endurance limit of GNG Cu can be enhanced by increasing the volume fraction of GNG surface layer, owing to the postponed onset of abnormal grain coarsening in a deeper subsurface layer and its longer propagation period to the top surface. Our finding points out a simple route to develop fatigue-resistant engineering structures through tailor-designing gradient nanostructures.

Acknowledgements

L.L. acknowledges the financial support by the National Science Foundation of China (Grant Nos. 51471172, 51420105001 and U1608257) and the key Research program of Frontier Science, CAS. The authors are grateful to Mr. X. Si for assistance in sample preparation.

References

[1] T.H. Fang, W.L. Li, N.R. Tao, K. Lu, Science 331 (2011) 1587–1590.
[2] X.L. Wu, P. Jiang, L. Chen, F.P. Yuan, Y.T.T. Zhu, Proc. Natl. Acad. Sci. U. S. A. 111 (2014) 7197–7201.
[3] Y. Wei, Y. Li, L. Zhu, Y. Liu, X. Lei, G. Wang, Y. Wu, Z. Mi, J. Liu, H. Wang, H. Gao, Nat. Commun. 5 (2014) 3580.
[4] T. Roland, D. Retraint, K. Lu, J. Lu, Scr. Mater. 54 (2006) 1949–1954.
[5] K. Dai, L. Shaw, Int. J. Fatigue 30 (2008) 1398–1408.
[6] L. Yang, N.R. Tao, K. Lu, L. Lu, Scr. Mater. 68 (2013) 801–804.
[7] H.W. Huang, Z.B. Wang, J. Lu, K. Lu, Acta Mater. 87 (2015) 150–160.
[8] J.Z. Long, Q.S. Pan, N.R. Tao, L. Lu, Scr. Mater. 145 (2018) 99–103.
[9] J.Z. Long, Q.S. Pan, N.R. Tao, L. Lu, Mater. Res. Lett. 6 (2018) 456–461.
[10] K. Lu, Nature. Rev. Mater. (2016) 16019.
[11] W.L. Li, N.R. Tao, K. Lu, Scr. Mater. 59 (2008) 546–549.
[12] R.Z. Valiev, R.K. Islamgaliev, I.V. Alexandrov, Prog. Mater. Sci. 45 (2000) 103–189.
[13] Y.S. Li, N.R. Tao, K. Lu, Acta Mater. 56 (2008) 230–241.
[14] S.R. Agnew, A.Y. Vinogradov, S. Hashimoto, J.R. Weertman, J. Electron. Mater. 28 (1999) 1038–1044.
[15] A. Vinogradov, S. Hashimoto, Mater. Trans. JIM 42 (2001) 74–84.
[16] H. Mughrabi, H.W. Höppel, M. Kautz, Scr. Mater. 51 (2004) 807–812.
[17] L. Kunz, P. Lukáš, M. Svoboda, Mater. Sci. Eng. A 424 (2006) 97–104.
[18] A.T. Winter, Philos. Mag. 30 (1974) 719–738.
[19] S. Suresh, Fatigue of Materials, 2nd ed Cambridge University Press, Cambridge, 1998.
[20] H. Mughrabi, Metall. Mater. Trans. B Process Metall. Mater. Process. Sci. 40 (2009) 431–453.
[21] S.D. Wu, Z.G. Wang, C.B. Jiang, G.Y. Li, I.V. Alexandrov, R.Z. Valiev, Scr. Mater. 48 (2003) 1605–1609.
[22] A. Pineau, A. Amine Benzerga, T. Pardoen, Acta Mater. 107 (2016) 508–544.
[23] H. Mughrabi, H.W. Höppel, Int. J. Fatigue 32 (2010) 1413–1427.